Revised Manuscript

Giant and Reversible Barocaloric Effect in Trinuclear Spin-Crossover Complex $Fe_3(bntrz)_6(tcnset)_6$

Michela Romanini,[1,*] YiXu Wang,[2,3,*] Kübra Gürpinar,[4] Gladys Ornelas,[2,5] Pol Lloveras,[6] Yan Zhang,[2] Wenkai Zheng,[7] Maria Barrio,[6] Araceli Aznar,[6] Adrià Gràcia-Condal,[1] Baris Emre,[8] Orhan Atakol,[4] Catalin Popescu,[9] Hu Zhang,[3] Yi Long,[3] Luis Balicas,[7] Josep Lluís Tamarit,[6] Antoni Planes,[1] Michael Shatruk,[2,7,†] and Lluís Mañosa[1,‡]

[1]*Departament de Física de la Matèria Condensada, Facultat de Física, Martí i Franquès 1, Universitat de Barcelona, 08028 Barcelona, Catalonia.*

[2]*Department of Chemistry and Biochemistry, Florida State University, Thallahassee, FL 32306, United Sates*

[3]*School of Materials Science and Engineering, University of Science and Technology Beijing, Beijing, 100083, P.R. China*

[4]*Department of Chemistry, Faculty of Science, Ankara University, Ankara 06100, Turkey*

[5]*G.W. Brackenridge High School, San Antonio, Texas, 78210, United Sates*

[6]*Grup de Caracterització de Materials, Departament de Física, EEBE and Barcelona Research Center in Multiscale Science and Engineering, Universitat Politècnica de Catalunya, Eduard Maristany, 10-14, 08019 Barcelona, Catalonia.*

[7]*National High Field Magnetic Laboratory, Tallahasse, FL 32310, United States*

[8]*Department of Engineering Physics, Faculty of Engineering, Ankara University, 06100 Ankara, Turkey.*

[9]*CELLS-ALBA Synchrotron, E-08290 Cerdanyola del Vallès, Catalonia, Spain*

(Dated: January, 3, 2021)

Abstract

We report a giant barocaloric effect (BCE) in a molecular material $Fe_3(bntrz)_6(tcnset)_6$ (**FBT**), where bntrz = 4-(benzyl)-1,2,4-triazole and tcnset = 1,1,3,3-tetracyano-2-thioethylepropenide. The crystal structure of **FBT** contains a trinuclear transition metal complex that undergoes an abrupt spin-state switching between the state in which all three Fe^{II} centers are in the high-spin (S = 2) electronic configuration and the state in which all of them are in the low-spin (S = 0) configuration. Despite the strongly cooperative nature of the spin transition, it proceeds with a negligible hysteresis and a large volumetric change, suggesting that **FBT** should be a good candidate for producing a large BCE. Powder X-ray diffraction and calorimetry revealed that the material is highly susceptible to applied pressure, as the transition temperature spans the range from 318 K at ambient pressure to 383 K at 2.6 kbar. Despite the large shift in the spin-transition temperature, its non-hysteretic character is maintained under applied pressure. Such behavior leads to a remarkably large and reversible BCE, characterized by the entropy change of 120 J kg^{-1} K^{-1} and the temperature change of 35 K, which are among the highest reversible values reported for any caloric material thus far.

1. Introduction.

Recent developments in solid-state cooling technologies have highlighted the need for discovering high-performance refrigerants that exhibit phase transitions associated with giant yet reversible isothermal entropy changes (ΔS) and adiabatic temperature changes (ΔT)[1,2]. Extensive research has shown that the caloric effects in solid-state materials can be triggered by various external stimuli that couple to at least one of the phase transition order parameters. For example, the magnetocaloric effect (MCE)[3,4] can be realized by applying magnetic field to impact the ordering of magnetic moments in the vicinity of the magnetic phase transition. Likewise, the electrocaloric effect (ECE)[5] is achieved as a response of electric dipoles to applied electric field in the vicinity of an electric phase transition. Another type of transitions with caloric effects is offered by mechanocaloric effects[6], which can be pronounced in the materials that exhibit high sensitivity to external stress fields, such as a uniaxial stress (the elastocaloric effects, eCE),[7,8] a hydrostatic pressure (the barocaloric effect, BCE),[9–11] or a combination of different stresses[12].

While the solid-state BCE offers a fundamentally important branch of mechanocaloric effects, at the earlier stage it was not recognized as a potentially powerful standalone phenomenon for application in refrigeration technologies.[13] Hydrostatic pressure used to be employed as an external stress field for enhancing the MCE in magnetic materials, with the idea that the applied pressure should strengthen the first-order character of the magnetic phase transition[14–17]. Nevertheless, the discovery of giant BCEs in well-known magnetocaloric materials, such as $Ni_{49.26}Mn_{36.08}In_{14.66}$,[18] $Gd_5Si_2Ge_2$,[19] $Fe_{49}Rh_{51}$,[20] $MnCoGe_{0.99}In_{0.01}$,[21] and $LaFe_{11.33}Co_{0.47}Si_{1.2}$ (inverse BCE),[22] suggested that substantial caloric effects can be achieved by application of hydrostatic pressure as an independent tuning parameter. There exists a fertile playground for discovering novel giant-BCE materials in diverse classes of compounds, both inorganic (e.g., AgI,[23] $(NH_4)_2SO_4$,[24] $(Pr_4N)[Mn(dca)_3]$ (Pr = propyl, dca = dicyanamide)[25]) and organic (e.g., neopentylglycol,[9,10] tris(hydroxymethyl)aminomethane[9] and fullerene C_{60}[26]).

Recently, spin-crossover (SCO) complexes have emerged as promising solid-state barocaloric refrigerants[27]. The SCO phenomenon is typically observed as switching between two electronic configurations of an octahedrally coordinated 3d metal ion (Fig. 1). The interconversion between the states with the minimum (low-spin, LS) and maximum (high-spin, HS) numbers of unpaired d-electrons can be triggered by changes in temperature, pressure,

or light irradiation[28]. The antibonding nature of e_g orbitals causes a pronounced weakening

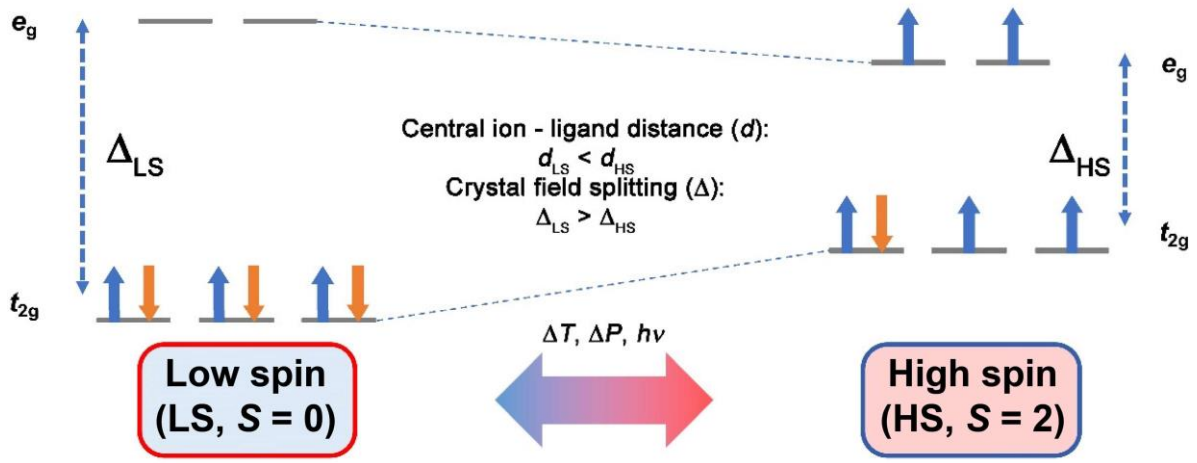

Fig. 1: Schematic illustration of SCO for a transition metal ion with d^6 electronic configuration. The transition can be induced by changes in temperature (ΔT), pressure (Δp) or light irradiation ($h\nu$).

and lengthening of the metal-ligand bonds in the HS state. The higher spin multiplicity ($2S+1$) and the shallower potential energy well of the HS state cause the increase in the magnetic and vibrational entropy that drives the LS → HS transition upon temperature increase[29]. In turn, an increase in pressure favors the lower-volume LS state and, in the case of an abrupt SCO transition, drives a substantial entropy decrease that can be harvested as a caloric effect[30].

Thus far, the number of studies of BCE in SCO materials have been rather scarce. An Ising-like microscopic model applicable to a one-dimensional SCO complex, $[Fe(hyptrz)_3](4\text{-}ClPhSO_3)_2\,H_2O$ (hyptrz = 4-(3'-hydroxypropyl)-1,2,4-triazole), had been established[30]. An isothermal entropy change as large as $\sim$ 60 J kg^{-1} K^{-1} and an adiabatic temperature change of $\sim$ 8 K were predicted, and those values were subsequently verified experimentally[31]. The SCO transition in the reported BCE complexes[31,32] has a relatively large hysteresis that imposes severe restrictions on the practical application of these materials as solid-state refrigerants due to the reduction in effective cooling power. Noteworthy, among a wealth of reported caloric materials, only a few exhibit both a large caloric effect and a negligible hysteresis under variable external field[26,33,34].

While the strongly hysteretic behavior is highly sought for applications of SCO materials in sensing, switching, and actuation, it is detrimental to caloric applications. The abruptness of SCO, however, is critical to maximizing the BCE. Therefore, one faces a non-trivial challenge to achieve the balance between the cooperativity of the spin transition, known to cause

the abrupt and often hysteretic behavior, and the rapid structural response to the external stimuli, with a minimal hysteresis. Fortunately, a number of SCO complexes that exhibit abrupt spin transitions with negligible hysteresis are already known, and it is of interest to explore their barocaloric properties. When analyzing a range of possible candidates for such studies, we identified a recently reported trinuclear complex $Fe_3(bntrz)_6(tcnset)_6$ (bntrz = 4-(benzyl)-1,2,4-triazole, tcnset = 1,1,3,3-tetracyano-2-thioethylpropenide) as a particularly promising material, since it exhibits an abrupt one-step spin transition near room temperature ($T_{½}$ = 318 K, where $T_{½}$ is the temperature at which the observed fractions of the HS and LS states are equal)[35]. Importantly, the transition occurs with negligible hysteresis, in contrast to strongly hysteretic spin transitions typically observed in related one-dimensional chain complexes in which Fe^{II} ions are bridged by triazole ligands[36].

Herein, we report a giant BCE in $Fe_3(bntrz)_6(tcnset)_6$ (**FBT**). We demonstrate that the robust BCE is achieved due to the preservation of the non-hysteretic character of the spin transition upon pressurization. The obtained entropy and temperature changes are amongst the largest reported values for any caloric material. These values are found to be reversible for low applied pressure, over a broad temperature range, underscoring the potential practical value of this barocaloric material.

2. Results and Discussion.

2.1. Synthesis, Structural and Magnetic Properties

Illustrative powder diffraction patterns (PXRD) are shown in Figs. 2 a-d. At room-temperature and atmospheric pressure the Pawley method resulted in a good agreement between the observed and calculated profiles (Fig. 2a) for the crystal structure of **FBT**. The lack of any additional peaks indicates phase purity of the sample. PXRD data at atmospheric

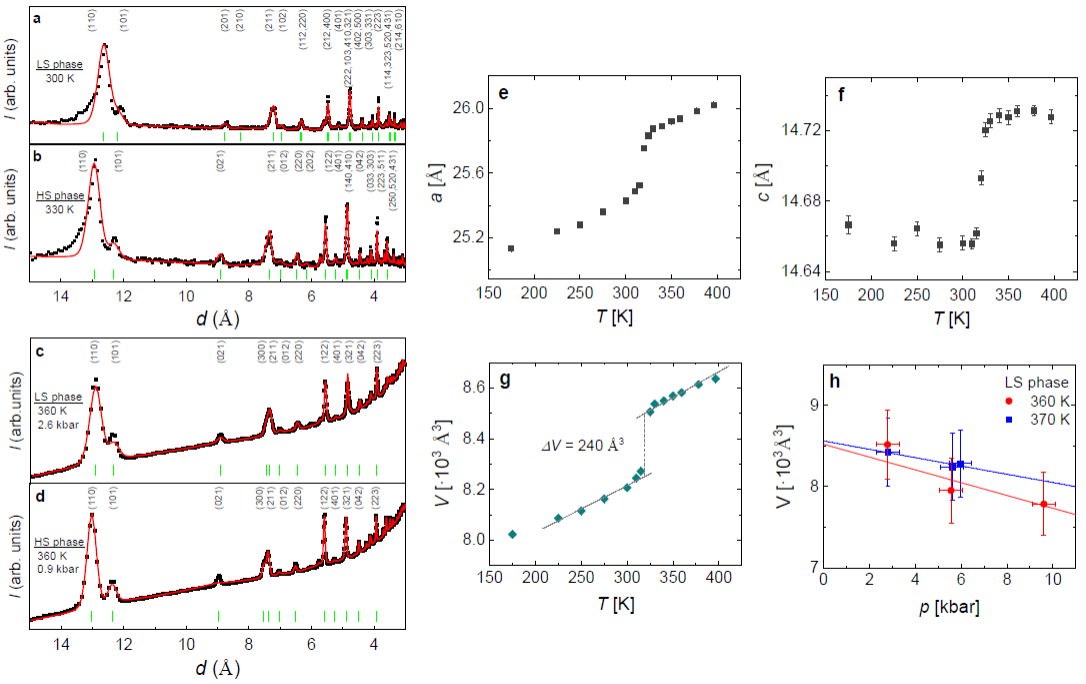

Fig. 2: Ambient pressure powder diffraction patterns at T = 300 K (a) and T = 330 K (b). Isothermal (T = 360 K) powder diffraction patterns at p = 2.6 kbar (c) and p = 0.9 kbar (d). Panels (a) and (c) correspond to the LS state and panels (b) and (d), to the HS state. Solid symbols correspond to experimental data, red lines are calculated patterns via *pattern matching fitting procedure, and green lines indicate the position of the Bragg peaks, whose* (hkl) *Miller indices are indicated on top of each panel. Ambient pressure temperature evolution of the lattice parameters (e) and (f), and of the unit cell volume (g). Pressure dependence of the unit cell volume at selected values of temperature (h). Lines are linear fits to the data.*

pressure correspond to the LS state at T = 300 K (Fig. 2a), and to the HS state at T = 330 K (Fig. 2b). Our results are in good agreement with the previous report,[35] as the two patterns can be indexed in the trigonal space group $R\bar{3}$ with lattice parameters a = 25.429(6) Å and c = 14.656(4) Å, and volume V = 8208(3) Å^3, for the LS state, and a = 25.831(6) Å and c = 14.720(4) Å and volume V = 8506(4) Å^3 for the HS state. Using the patterns recorded at selected temperatures we have determined the temperature dependence of the unit cell parameters and volume (Figs. 2 e-g), which exhibit a sharp change at the SCO transition. The volume thermal expansion in the vicinity of the SCO transition is $\beta = (2.5 \pm 0.4) \cdot 10^{-4}$ K^{-1} for the HS state, and $\beta = (2.7 \pm 0.4) \cdot 10^{-4}$ K^{-1} for the LS state, and the

volume change at the SCO transition is $\Delta V = 240$ Å^3. Pressure-dependent PXRD patterns collected at $T = 360$ K revealed the LS state at $p = 2.6$ kbar (Fig. 2c) and the HS state at $p = 0.9$ kbar (Fig. 2d). Using the PXRD patterns recorded at 360 K and 370 K, at different values of hydrostatic pressure, we computed the pressure dependence of the unit cell volume of the LS phase (Fig. 2h). Despite the considerable scatter of the data, it is possible to estimate rough values for the isothermal compressibility as $\kappa \sim 0.09$ GPa^{-1} at $T = 360$ K and $\kappa \sim 0.06$ GPa^{-1} at $T = 370$ K. The bulk moduli (B) derived from these values compare well with reported data for the LS phase in related SCO compounds[37]. For the studied temperature region, the narrow pressure range of stability of the HS phase did not allow us to obtain reliable PXRD data at different values of applied hydrostatic pressure.

The product of magnetic susceptibility (χ) by temperature (Fig. 3a) showed a value of 11.5 emu K mol^{-1} at 380 K. The value of χT for a single HS Fe^{II} ion ($S = 2$) is usually in the range of 3.3-3.8 emu K mol^{-1} (the deviation from the spin-only χT value of 3.0 emu K mol^{-1} is explained by a slight orbital contribution)[38]. Hence, the total χT value observed for **FBT** at 380 K is in agreement with the presence of three HS Fe^{II} ions, and the effect of magnetic exchange between the Fe^{II} centers is negligible at this temperature. As the temperature is lowered, the χT product exhibits a dramatic decrease to values close to 0, indicating the complete spin transition to the state that contains only LS Fe^{II} ions (S = 0). The midpoint of this transition corresponds to $T_{½}$= 318 K, in agreement with the previous report[35]. Additionally, the SCO transition showed excellent reversibility, with the hysteresis width of only $\sim$ 1 K, which is very narrow compared to the majority of SCO materials that exhibit abrupt transitions,[34,39,40,41] including those for which giant BCEs have been reported[31,32]. The negligible thermal hysteresis accompanying the spin transition in **FBT** provides an ideal scenario to fully exploit the cooling capacity of this material in a barocaloric cycle.

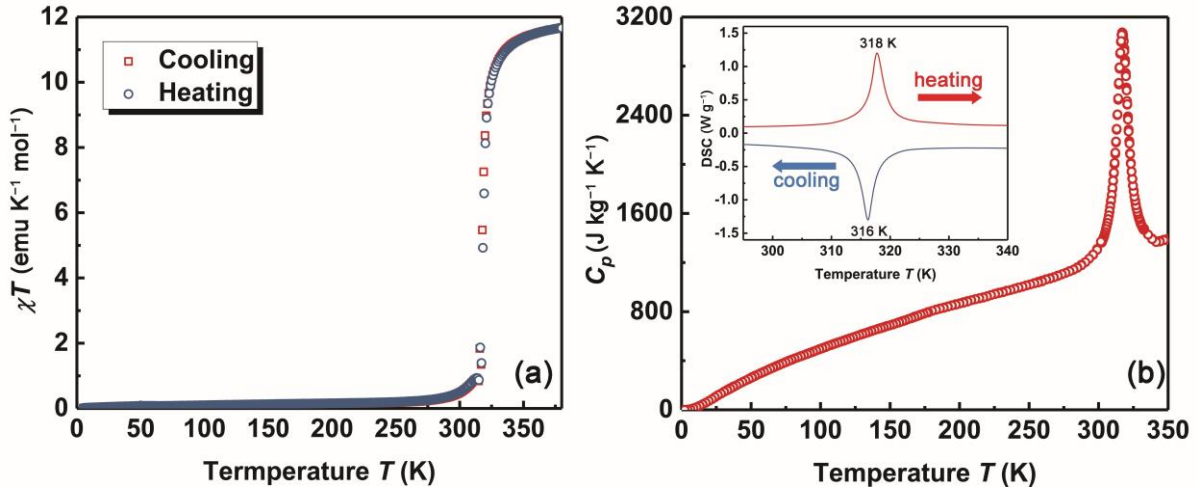

Fig. 3: a) Magnetic susceptibility data as a function of temperature. (b) Specific heat as a function of temperature. The inset shows differential scanning calorimetry curves where the upper and lower curves correspond, respectively, to the endothermal LS to HS transition on heating and to the exothermal HS to LS transition on cooling.

The thermal effects accompanying the SCO transition in **FBT** were elucidated by differential scanning calorimetry (DSC) and specific heat measurements (Fig. 3b). DSC curves (inset in Fig. 3b) revealed a large peak associated with the SCO transition in both the heating and cooling regimes. The peak positions, usually taken as the phase transition temperature, were 318 K and 316 K, respectively. Experiments carried out at different heating and cooling rates (2, 4 and 10 K min^{-1}) confirmed a small hysteresis of 2 K. The slightly larger hysteresis width observed in DSC measurement is explained by the larger temperature variation rate as compared to the rate used in magnetic measurements (1 K min^{-1}). After subtracting the baselines, the peak areas were integrated to obtain the enthalpy of the transition (ΔH_t), and the entropy of the transition was computed as $\Delta S_t = \int_{T_1}^{T_2} \frac{1}{T}\frac{dQ}{dT}\,dT$, where $\frac{dQ}{dT} = \frac{\dot{Q}}{|\dot{T}|}$ and T_1 and T_2 are the start and the end temperatures of the SCO transition, respectively. ΔH_t and ΔS_t values were found to be coincident for heating and cooling runs, within experimental errors. By averaging over all runs we have obtained ΔH_t = 25 ± 2 kJ kg^{-1} and ΔS_t = 80 ± 5 J kg^{-1} K^{-1}.

The temperature dependence of specific heat (see Fig. 3b) exhibits an apparent peak at the SCO transition due to the latent heat. The entropy change at the SCO transition consists of two major contributions, associated with magnetic (ΔS_m) and lattice (ΔS_v) effects. The magnetic contribution to this entropy change can be estimated as $\Delta S_m = R \ln\left(\frac{\Omega_{HS}}{\Omega_{LS}}\right)$ where Ω_{HS} and Ω_{LS} are, respectively, the spin multiplicity for the HS and LS states, and R is the gas constant. For the linear trimer of three Fe^{II} ions, S=2 for each ion, and the spin multiplicity

in the HS phase is equal to $(2S + 1)^3$=125. Assuming that the transition to the S=0 LS state is essentially complete, we obtain ΔS_m = 40 J K^{-1} mol^{-1} = 17 J kg^{-1} K^{-1} (where a molecular weight M=2330 g mol^{-1} has been taken[35]. This value can be assumed to be an upper limit since assumes no interactions between the spins in the trinuclar complex. However, it is well known that the coupling between spins in these materials becomes pronounced only at lower temperatures, below 50 K, but at those temperatures our material is already in the low-spin (S=0) state. The effect of magnetic exchange in the present compound around the spin transition temperature is negligilbe. In common with many other compounds, the entropy at the SCO transition in **FBT** is dominated by lattice effects, which can be estimated as $\Delta S_v = \Delta S_t - \Delta S_m$ = 63 J kg^{-1} K^{-1}. On the other hand, the lattice contribution can be estimated from the volume change at the phase transition, the thermal expansion and isotherml compressibility as, $\Delta S_v = \frac{\bar{\beta}}{\bar{\kappa}} \Delta V$, where $\bar{\beta}$ and $\bar{\kappa}$ are the averaged values of thermal expansion and isothermal compressibility of the two phases close to the transition[42]. Under the assumption that the compressibility in the HS state will not significantly differ from that in the LS state[37], and using the data derived from PXRD experiments (ΔV = 240 $Å^3$ = 2.05 · 10^{-5} m^3 kg^{-1}, $\bar{\beta}$ = 2.6 · 10^{-4} K^{-1}, and $\bar{\kappa}$= 0.08 GPa^{-1}) we obtain $\Delta S_v \cong$ 64 J kg^{-1} K^{-1}, in a very good agreement with the values derived from DSC data and magnetic estimates.

2.2 High-Pressure Calorimetry Studies

To determine the BCE associated with the SCO transition we have performed calorimetry under variable hydrostatic pressure. The base-line corrected thermal curves ($\frac{dQ}{dT}$) recorded on heating and cooling the sample through the SCO transition are plotted in Fig. 4a as a function of temperature for selected values of the applied pressure. Although no systematic study of the stability with cycling has been performed, results were found to be reproducible after about one hundred cycles.

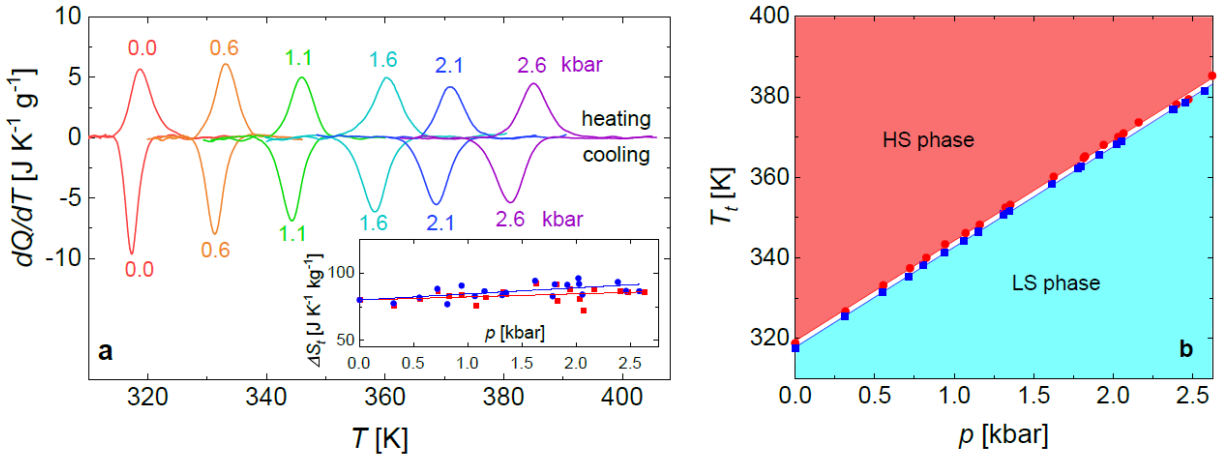

Fig. 4: (a) Temperature-dependent isobaric heat flow dQ/dT at different pressures, after baseline subtraction. The upper and lower curves correspond, respectively, to the endothermal LS to HS transition on heating and to the exothermal HS to LS transition on cooling. The inset shows the transition entropy change as a function of pressure. Blue symbols correspond to the HS to LS transition and red symbols, to the LS to HS transition. (b) Transition temperature (peak in the calorimetric cirves) as a function of hydrostatic pressure. Blue symbols correspond to the HS to LS transition and red symbols, to the LS to HS transition. Lines are linear fits to the data.

The endothermal and exothermal peaks, associated, respectively, with the LS to HS and HS to LS transitions, shift to higher temperatures with increasing hydrostatic pressure. This behaviour is consistent with pressure stabilizing the low volume LS phase and suggests a conventional BCE for compound **FBT**. The increase in the transition temperature, taken as the temperature of the peak in the calorimetric curves, is linear with a slope dT/dp = 25.0 ± 0.2 K kbar^{-1} for both the LS to HS transition and the HS to LS transition (Fig. 4b). This value matches with the value computed from the Clausius-Clapeyron equation $\frac{dT}{dp} = \frac{\Delta V}{\Delta S_t} = 25.6\ K \cdot kbar^{-1}$. The similarity in the dT/dp values for the forward and reverse transitions implies that the hysteresis of the spin transition is not affected by hydrostatic pressure, as illustrated in Fig. 4b. Inducing the transition by applying and removing pressure results in a very low hysteresis Δp ~ 65 bar. By integrating the calorimetric curves we have obtained the values for ΔS_t as a function of pressure, shown in the inset of Fig. 4a. Although a slight tendency of $|\Delta S_t|$ to increase with increasing pressure cannot be discarded, ΔS_t can be considered to be pressure independent within experimental errors. This result is in contrast to the behaviour found for one-dimensional chain complexes where $|\Delta S_t|$ decreases with increasing pressure[32] (with the associated reduction in the barocaloric performances of the compound).

The combination of specific heat data with the pressure-dependent thermal curves enables to determine the entropy, referenced to a value at a given temperature (T_0) and atmospheric pressure, as:

$$S'(T,p) = \begin{cases} \int_{T_0}^{T} \frac{C_p^{LS}}{T} dT & T \le T_1 \\ S'(T_1,p) + \int_{T_1}^{T} \frac{1}{T}\left(C_p + \frac{dQ}{dT}\right) dT & T_1 < T \le T_2 \\ S'(T_2,p) + \int_{T_2}^{T} \frac{C_p^{HS}}{T} dT & T_2 < T \end{cases} \quad (1)$$

where T_1 and T_2 are the start and end temperatures of the SCO transition. C_p^{LS} and C_p^{HS} are specific heats of the LS and HS states, respectively, and $C_p = xC_p^{LS} + (1-x)C_p^{HS}$ where x is the fraction of the sample in the LS state. Equation (1) is computed by assuming pressure independent specific heats, which is a good approximation, taking into account the relatively narrow temperature interval over which it is computed. Nevertheless, the contribution to the entropy ($\Delta S_+(T_0, p)$) arising from the pressure dependence of the specific heat over a broad temperature range from zero to T_0 cannot be neglected for compressible organic and metal-organic materials. Such a contribution can be computed as:

$$\Delta S_+(T_0,p) = S(T_0,p) - S(T_0,p_{atm}) = \int_0^{T_0} \frac{C_p(T,p) - C_p(T,p_{atm})}{T} dT \cong -\left(\frac{\partial V}{\partial T}\right)_p \Delta p \quad (2)$$

with $\Delta p = (p - p_{atm}) \cong p$, and where $\left(\frac{\partial V}{\partial T}\right)_p$ is evaluated at $p_{atm} = 1$ atm, and it is assumed to be pressure independent.

Using the specific heat data at atmospheric pressure (Fig. 3b), the thermal curves at selected values of pressure (Fig. 4a), and the thermal expansion (Fig. 2g), we have computed the entropy curves $S(T,p) = S'(T,p) + \Delta S_+(T_0,p)$ as a function of temperature for selected values of applied pressure (Figs. 5a and 5b). From these entropy curves it is straightforward to compute the isothermal entropy change induced by the application of a pressure p as:

$$\Delta S(T, 0 \rightarrow p) = S(T,p) - S(T,0), \quad (3)$$

and the adiabatic temperature change as:

$$\Delta T(S, 0 \rightarrow p) = T(S,p) - T(S,0) \quad (4)$$

For a release of pressure ($p \rightarrow 0$), equivalent expressions hold.

Results for ΔS and ΔT upon the first application ($0 \rightarrow p$) and first removal ($p \rightarrow 0$) of

pressure are shown in Figs. 5c and 5d, and 5e and 5f, respectively (where we have taken T_0 = 250 K). Because application of pressure promotes the HS to LS (exothermal) transition, $\Delta S(0 \rightarrow p)$ and $\Delta T(0 \rightarrow p)$ curves were computed from the entropy curves obtained from the calorimetric runs on cooling (Fig. 5a). Conversely, $\Delta S(p \rightarrow 0)$ and $\Delta T(p \rightarrow 0)$ curves were computed from the entropy curves obtained from the calorimetric runs on heating (Fig. 5b). A salient feature found from the data shown in Fig. 5 is the large values for both ΔS and ΔT, for all ranges of applied pressures. Noticeably, for low values of applied pressure (p = 0.33 kbar), entropy and temperature changes have outstanding values of ΔS = 80 J kg^{-1} K^{-1} and $\Delta T \sim$ 6 K, and they increase up to ΔS = 120 J kg^{-1} K^{-1} and ΔT = 35 K for an applied pressure of p = 2.6 kbar. These values are amongst the largest reported for barocaloric materials. The major contribution to ΔS is due to the transition entropy change (ΔS_t) of the SCO. The fact that for the lowest applied pressure $\Delta S \approx \Delta S_t$ indicates that only very small pressure is required to induce the full HS to LS transition, thanks to the sharpness of the thermal SCO transition and the high sensitivity of the transition temperature to pressure. As pressure increases, there is an increasing contribution from ΔS_+, which reaches about one third of the total ΔS value for an applied pressure of 2.6 kbar.

The reversibility of the BCE upon pressure cycling is a key factor for a practical application of the BC material in a refrigeration device. In Fig. 6, we show the reversible isothermal entropy (ΔS_{rev}) and adiabatic temperature (ΔT_{rev}) changes computed following the procedures described elsewhere[23,27]. The negligible hysteresis of the spin transition in **FBT**, added to the strong sensitivity of the transition to pressure, results in a very large reversible BCE for the entire studied range of applied pressures. Importantly, the giant and reversible BCEs extend over a large temperature window (T_{span}), which is a pre-requisite for designing cooling devices with a broad operational temperature range. Other figures of merit commonly used to characterize the suitability of caloric materials for cooling devices are the Refrigerant Capacity (RC), which corresponds to the area below the peak (or plateau) in the ΔS_{rev} vs T curves (Fig. 6a), and the Coefficient of Refrigerant Performance (CRP) which is defined as CRP = | ΔT_{rev} ΔS / W|, where W is the work required to reversibly drive the caloric effect, which for barocaloric materials can be computed as $W = \frac{1}{2} p \Delta V$. For **FBT**, RC = 564 J kg^{-1} at p= 0.3 kbar and it increases up to RC = 5800 J kg^{-1} at p= 2 kbar, and CRP varies between 1.5 and 1.8 over all the studied pressure range. The values for these figures of merit are among the largest reported values for giant and colossal caloric materials [26,43].

In Table I, the barocaloric performance of **FBT** is compared to those of the one-dimensional

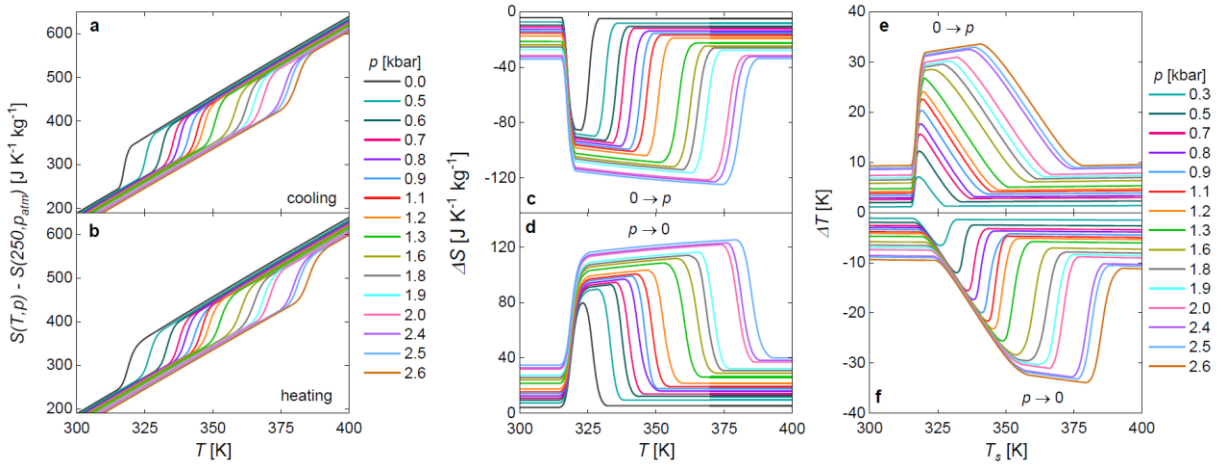

Fig. 5: Temperature-dependent isobaric entropy curves at different pressures on cooling (a) and heating (b). Barocaloric isothermal entropy change corresponding to the first application (c) and first removal (d) of pressure. Barocaloric adiabatic temperature change corresponding to the first application (e) and first removal (f) of pressure. The pressure values are indicated by the same colour code in all panels.

chain SCO compound and the best BCE materials reported so far. We have not included metallic alloys since they exhibit lower values for ΔS and ΔT. The reversible ΔS and ΔT found for **FBT** are significantly larger than the (irreversible) values previously reported for other SCO compounds[32]. Compared to the recently reported colossal BCE in plastic crystals[9,10,44], **FBT** exhibits lower ΔS but about double ΔT values. These larger ΔT are due to the negligible hysteresis of the SCO transition. Indeed, as illustrated in Table I, adiabatic temperature changes in **FBT** represent the largest reported values for any barocaloric material, and they compare well to the values reported for colossal elastocaloric alloys[8].

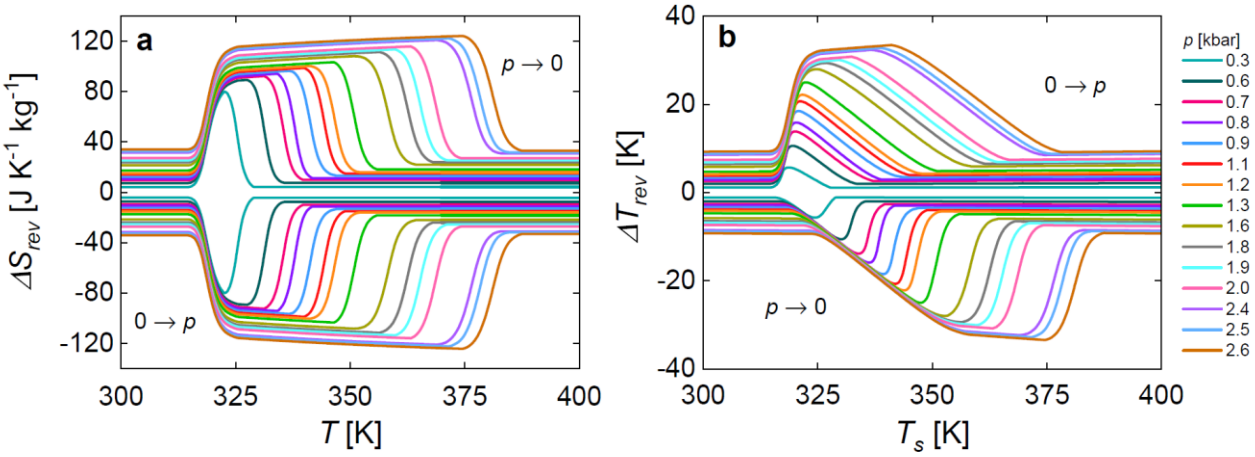

Fig. 6 (a) Reversible isothermal entropy changes on decompression and compression as a function of temperature at different pressures. (b) Reversible adiabatic temperature changes on decompression and compression as a function of temperature at different pressures.

3. Conclusion

In summary, we have reported giant barocaloric effects in a trinuclear spin crossover compound. The giant values for the isothermal entropy change and adiabatic temperature change have been found to be reversible at low pressures. The adiabatic temperature changes found for the title SCO coordination compound are larger than the values reported for any barocaloric material up to date. In fact, they compare well with the colossal elastocaloric data which are the largest reversible changes found for any caloric material so far. We expect that present results will stimulate further research into the barocaloric effects observed in spin-crossover materials, especially in terms of identifying the design principles that could lead to abrupt yet non-hysteretic spin transitions, which remain robust under applied pressure while demonstrating the high sensitivity of the transition temperature to pressure.

Table I: Compound, dT/dp, pressure change Δp, reversible entropy ΔS_{rev} and temperature ΔT_{rev} changes, temperature window (T_{span}), and hysteresis (ΔT_{hyst}). Values indicated with * refer to irreversible data. For those compounds with different dT/dp on heating and cooling, the approximate average value is given. Data for hysteresis are at atmospheric pressure.

Sample	$\left\|\frac{dT}{dp}\right\|$	Δp	$\lvert\Delta S_{rev}\rvert$	$\lvert\Delta T_{rev}\rvert$	T_{span}	ΔT_{hyst}	Reference
	(K kbar^{-1})	(kbar)	(J kg^{-1} K^{-1})	(K)	(K)	(K)	
$Fe_3(bntrz)_6(tcnset)_6$	25	0.55	80	10	10	2	This work
		2.6	120	35	50	2	This work
$[FeL_2](BF_4)_2$	15	0.43	68(*)	4(*)	-	4	[32]
$(NH_4)_2SO_4$	~5	1	60	-	~5	~6	[24]
AgI	~14	2.5	60	18	~20	25	[23]
(TPrA)[Mn(dca)$_3$]	23	0.07	31	5	1	~1	[25]
		1	31	5	20	–	[25]
C_{60}	17	1	32	10	10	3	[27]
		4.1	42	16	70	3	[27]
$(CH_3)_2C(CH_2OH)_2$	~12	0.9	380(*)	–	–	~15	[9]
$(CH_3)C(CH_2OH)_3$	8	2.4	490	10	~10	~4	[44]
$(CH_3)_3C(CH_2OH)$	22	2.6	320	16	~40	~24	[44]

Experimental and Methods

A. Synthesis

All reactions were performed in an inert atmosphere using standard Schlenk techniques. All reagents were obtained commercially from Millipore Sigma and Acros and used without further purification. Anhydrous commercial solvents were additionally purified by passing through a double-stage drying/purification system (Glass Contour Inc.). Distilled water was purged with dry N_2 gas for 30 min prior to use. The complex $Fe_3(bntrz)_6(tcnset)_6$ (**FBT**) was

synthesized according to the published procedure[35]. A polycrystalline sample of 1 g in total mass was produced by layering a solution of bntrz in methanol on top of an aqueous solution of K(tcnset) and $Fe(BF_4)_2\,6H_2O$ in a custom-made 300 mL Schlenk tube. A pink microcrystalline powder of **FBT** that accumulated after 3 days was recovered by filtration, washed with methanol and diethyl ether, and dried by suction. The compound is air-stable and can be stored in closed vials for more than a year without any change. While SCO materials with abrupt spin transition frequently show cracking of single crystals when going through the phase transition, this is not a problem with the powdered samples that were used in our studies.

B. Magnetic Measurements

Magnetic measurements were performed with a Quantum Design SQUID magnetic property measurement system (MPMS). A sample of FBT with a mass of ~ 20 mg was tightly packed in a polycarbonate capsule and placed inside a vertical plastic straw that was suspended in the MPMS sample chamber. DC magnetic susceptibility was measured in the temperature range of 5-380 K at a scan rate of 1 K min^{-1} and applied magnetic field of 1000 Oe. Additional background signal data were collected for diamagnetic corrections.

C. X-ray Diffraction

The phase purity of the sample was verified by PXRD measurements performed at room temperature and atmospheric pressure on a lab-scale Rigaku SmartLab SE diffractometer equipped with a Cu-Kα radiation source (λ = 1.54187 Å). PXRD experiments at various temperatures and atmospheric pressure were carried out using an INEL diffractometer with Cu-Kα_1 radiation (λ = 1.54187 Å), a curved position-sensitive detector (CPS120), a 0.5-mm-diameter Lindemann capillary and a 700 series Oxford Cryostream Cooler to control the temperature. PXRD experiments at various temperatures and pressures were carried out at the ALBA-CELLS synchrotron light source[45]. Data were collected at beamline MPSD BL04 using a monochromatic beam (λ = 0.4246 Å) focussed down to 20 × 20 μm^2 (FWHM). The sample-to-detector distance (380 mm) and the beam center position were calibrated from LaB_6 diffraction measured in the same conditions as the sample. Angle-dispersive XRD measurements at high temperature were performed in a gas-membrane driven diamond anvil

cell (DAC). PXRD data was studied by Pawley method using the FullProf Suite program[46]. The sample temperature was controlled by a combination of a resistive heater and a K-type thermocouple. Pressure was determined using both NaCl equation of state[47] and Sm:SrB_4O_7 fluorescence method[48].

D. Thermal Property Measurements

DSC measurements were performed on a sample of ~ 2 mg using a TA instruments Q100 differential scanning calorimeter at the scanning rates of 2, 4 and 10 K min^{-1}. The heat capacity data were collected in the temperature range from 2 to 350 K, using the Physical Property Measurement System (Quantum Design). Apiezon-N® grease was used to thermally couple the **FBT** sample to the platform of the calorimeter. The sample with the mass of 2.477 mg was in the form of a pellet with 3 mm in diameter and 0.5 mm thickness. The standard relaxation time technique was used to extract the heat capacity. The contribution of the platform, including the grease, was measured independently and subtracted from the total heat capacity data. High- pressure thermal measurements were conducted using a customized calorimeter consisting of a metallic block and Bridgman-type seals, operating from room temperature to 473 K. Heating ramps were performed by means of a resistive heater and an external controller, whereas cooling was carried out by means of air stream. A ~ 200 mg mass polycrystalline sample of **FBT** was mixed with an inert perfluorinated liquid (Galden Bioblock Scientist) to remove air and sealed in tin capsules. The pressure transmitting liquid was Therm-240 (from Lauda).

Acknowledgements

This research was supported by the MINECO (Spain) under projects no. MAT2016-75823-R, FIS2017-82625-P and FIS2017-83295-P, the DGU (Catalonia) project 2017SGR-42, by the US National Science Foundation (award CHE-1955754 to M.S.), by the US Department of Energy Basic Energy Sciences program (award DE-SC0002613 to L.B.) and by Scientific and Technological Research Council of Turkey (TÜBITAK), Grant No: MFAG-118F128. Y. X. W. acknowledges the Chinese Scholarship Council for supporting his visit to Florida State University (award No. 201706460046). G.O. was supported by the Research Experience for Teachers program administered by the National High Magnetic Field Laboratory, which is supported by the National Science Foundation Cooperative Agreement No.

DMR-1644779 and the state of Florida. A.G. acknowledges financial support from Universitat de Barcelona under the APIF scholarship. Powder X-ray diffraction experiments were performed at the MSPD beamline of Alba Synchrotron (experiment no. 2019093715).

---

* These two authors contributed equally to this work

† Electronic address: mshatruk@fsu.edu

‡ Electronic address: lluis.manosa@fmc.ub.edu

1 L. Mañosa, A. Planes, M. Acet, *J. Mater. Chem. A*, **2013**, 1, 4925.

2 X. Moya, S. Kar-Narayan, N.D. Mathur, *Nat. Mater.* **2014**, 13, 439.

3 J. Y. Law, V. Franco, L. M. Moreno-Ramírez, A. Conde, D. Y. Karpenkov, I. Radulov, K. P. Skokov, O. Gutfleisch, *Nat. Commun.*, **2018**, 9, 2680.

4 F. Guillou, F. Wilhelm, O. Tegus, A. Rogalev, *Appl. Phys. Lett.*, **2016**, 108, 122405.

5 E. Defay, R. Faye, G. Despesse, H. Strozyk, D. Sette, S. Crossley, X. Moya, N. D. Mathur, *Nat. Commun.*, **2018**, 9, 1827.

6 L. Mañosa, A. Planes, *Adv. Mater.*, **2017**, 29, 1603607.

7 H. Hou, E. Simsek, T. Ma, N. S. Johnson, S. Qian, C. Cissé, D. Stasak, N. Al Hasan, L. Zhou, Y. Hwang, R. Radermacher, V. I. Levitas, M. J. Kramer, M. A. Zaeem, A. P. Stebner, R. T. Ott, J. Cui, I. Takeuchi, *Science*, **2019**, 366, 1116.

8 D.Y. Cong, W.X. Xiong, A. Planes, Y. Ren, L. Mañosa, P.Y. Cao, Z.H. Nie, X.M. Sun, Z. Yang, X.F. Hong et al, . *Phys. Rev. Lett.*, **2019**, 122, 255703.

9 B. Li, Y. Kawakita, S. Ohira-Kawamura, T. Sugahara, H. Wang, J.F. Wang, Y.N. Chen, S.I. Kawaguchi, S. Kawaguchi, K. Ohara, et al. *Nature*, **2019**, 567, 506.

10 P. Lloveras, A. Aznar, M. Barrio, P. Negrier, C. Popescu, A. Planes, L. Mañosa, E. Stern-Taulats, A. Avramenko, N.D. Mathur et al. *Nat. Commun.*, **2019**, 10, 1803.

11 A. Aznar, P. Lloveras, J.-Y. Kim, E. Stern-Taulats, M. Barrio, J. L. Tamarit, C. F. Sánchez-Valdés, J. L. Sánchez Llamazares, N. D. Mathur, X. Moya, *Adv. Mater.*, **2019**, 31, 1903577.

12 R. Wang, S. Fang, Y. Xiao, E. Gao, N. Jiang, Y. Li, L. Mou, Y. Shen, W. Zhao, S. Li, A. F. Fonseca, D. S. Galvão, M. Chen, W. He, K. Yu, H. Lu, X. Wang, D. Qian, A. E. Aliev, N. Li, C. S. Haines, Z. Liu, J. Mu, Z. Wang, S. Yin, M. D. Lima, B. An, X. Zhou, Z. Liu, R. H. Baughman, *Science*, **2019**, 366, 216.

13 K. Alex Müller, F. Fauth, S. Fischer, M. Koch, A. Furrer, P. Lacorre, *Appl. Phys. Lett.*, **1998**, 73, 1056.

14 H. Yamada, K. Fukamichi, T. Goto, *Phys. Rev. B*, **2001**, 65, 024413.

15 S. Gama, A. A. Coelho, A. de Campos, A. M. G. Carvalho, F. C. G. Gandra, P. J. von Ranke, N. A. de Oliveira, *Phys. Rev. Lett.*, **2004**, 93, 237202.

16 Y. Sun, Z. Arnold, J. Kamarad, G.-J. Wang, B.-G. Shen, Z.-H. Cheng, *Appl. Phys. Lett.*, **2006**, 89, 172513.

17 L. Morellon, Z. Arnold, C. Magen, C. Ritter, O. Prokhnenko, Y. Skorokhod, P. A. Algarabel, M. R. Ibarra, J. Kamarad, *Phys. Rev. Lett.*, **2004**, 93, 137201.

18 L. Mañosa, D. Gonzàlez-Alonso, A. Panes, E. Bonnot, M. Barrio, J.-L. Tamarit, S. Aksoy, M. Acet, *Nat. Mater.* **2010**, 9, 478.

19 S. Yuce, M. Barrio, B. Emre, E. Stern-Taulats, A. Planes, J.-L. Tamarit, Y. Mudryk, K. A. Gschneidner, V. K. Pecharsky, L. Mañosa, *Appl. Phys. Lett.*, **2012**, 101, 071906.

20 E. Stern-Taulats, A. Planes, P. Lloveras, M. Barrio, J.-L. Tamarit, S. Pramanick, S. Majumdar, C. Frontera, L. Mañosa, *Phys. Rev. B*, **2014**, 89, 214105.

21 R.-R. Wu, L.-F. Bao, F.-X. Hu, H. Wu, Q.-Z. Huang, J. Wang, X.-L. Dong, G.-N. Li, J.-R. Sun, F.-R. Shen, T.-Y. Zhao, X.-Q. Zheng, L.-C. Wang, Y. Liu, W.-L. Zuo, Y.-Y. Zhao, M. Zhang, X.-C. Wang, C.-Q. Jin, G.-H. Rao, X.-F. Han, B.-G. Shen, *Sci. Rep.* ,**2015**, 5, 18027.

22 L. Mañosa, D. González-Alonso, A. Planes, M. Barrio, J.L. Tamarit, I.S. Titov, M. Acet, A. Bhattacharyya, S. Majumdar, *Nat. Commun.*, **2011**, 2, 595.

23 A. Aznar, P. Lloveras, M. Romanini, M. Barrio, J.-L. Tamarit, C. Cazorla, D. Errandonea, N. D. Mathur, A. Planes, X. Moya, L. Mañosa, *Nat. Commun.*, **2017**, 8, 1851.

24 P. Lloveras, E. Stern-Taulats, M. Barrio, J.-L. Tamarit, S. Crossley, W. Li, V. Pomjakushin, A. Planes, L. Mañosa, N.D. Mathur, X. Moya, *Nat. Commun.*, **2015**, 6, 8801

25 J. M. Bermúdez-García, M. Sánchez-Andújar, S. Castro-García, J. López-Beceiro, R. Artiaga, M. A. Señarís-Rodríguez, *Nat. Commun.*, **2017**, 8, 15715.

26. J. Li, D. Dunstan, X. Lou, A. Planes, L. Mañosa, M. Barrio, J.L. Tamarit, P. Lloveras, *J. Mater. Chem. A*, **2020**, 8, 20354.

27 K. G. Sandeman, *APL Materials*, **2016**, 4, 111102.

28. P. Gütlich, H. A. Goodwin, *Top. Curr. Chem.*, **2004**, 233, 1.

[29] A. Hauser, *Top. Curr. Chem.*, **2004**, 233, 49-58.

[30] P. J. von Ranke, *Appl. Phys. Lett.*, **2017**, 110, 181909.

31 P.J. von Ranke, B.P. Alho, R.M. Ribas, E.P. Nobrega, A. Caldas, V.S.R. de Sousa, M.V. Colaço, L. F. Marques, D.L. Rocco, P.O. Ribeiro, *Phys. Rev. B*, **2018**, 98, 224408.

32 S.P. Vallone, A.N. Tantillo, A.M. dos Santos, J.J. Molaison, R. Kulmaczewski, A. Chapoy, P. Ahmadi, M.A. Halcrow, K.G. Sandeman, *Adv. Mater.*, **2019**, 31, 1807334.

33 F. Guillou, A. K. Pathak, D. Paudyal, Y. Mudryk, F. Wilhelm, A. Rogalev, V. K. Pecharsky, *Nat. Commun.*, **2018**, 9, 2925.

34 M. Shatruk, H. Phan, B. A. Chrisostomo, A. Suleimenova, *Coord. Chem. Rev.***2015**, 289, 62.

35 N. Pittala, F. Thétiot, C. Charles, S. Triki, K. Boukheddaden, G. Chastanet, M. Marchivie, *Chem. Commun.*, **2017**, 53, 8356.

36 Y. Garcia, V. Niel, M. C. Muñoz, J. A. Real, *Top. Curr. Chem.*, **2004**, 233, 229.

37 M. Mikolasek, M.D. Manrique-Juárez, H.J. Sheperd, K. Ridier, S. Rat, V. Shalabaeva, A.C. Bas, I.E. Collings, F. Mathieu, J. Cacheux, T. Leichle, L. Nicu, W. Nicolazzi, L. Salmon, G. Molnár, A. Bousseksou, *J. Am. Chem. Soc.*, **2018**, 148, 8970.

38 M. Shatruk, A. Dragulescu-Andrasi, K. E. Chambers, S. A. Stoian, E. L. Bominaar, C. Achim, K. R. Dunbar, *J. Am. Chem. Soc.*, **2007**, 129, 6104.

39 M. A. Halcrow, *Polyhedron*, **2007**, 26, 3523.

40 P. Chakraborty, C. Enachescu, C. Walder, R. Bronisz, A. Hauser, *Inorg. Chem.*, **2012**, 51, 9714.

41 S. Brooker, *Chem. Soc. Rev.*, **2015**, 44, 2880.

42 R. Sandrock, G.M. Schneider, *Ber. Bunsenges. Phys. Chem.*, **1983**, 87, 197.

43 L. Mañosa, A. Planes, Appl. Phys. Lett. **2020**, 116, 050501; **2020**, 116, 099901.

44 A. Aznar, P. Lloveras, M. Barrio, P. Negrier, A. Planes, L. Mañosa, N.D. Mathur, X. Moya, J.L. Tamarit, *J. Mater. Chem. A*, **2020**, 8, 639.

45 F. Fauth, I. Peral, C. Popescu, M. Knapp, *Powder Diffraction*, **2013**, 28, S360.

46 https://www.ill.eu/sites/fullprof/

47 P.I. Dorogokupets, A. Dewaele, *High Press. Res.*, **2007**, 27, 431.

48 S.V. Raschenko, A. Kurnosov, I. Dubrovinsky, K. Litasov, *J. Appl. Phys.*, **2015**, 117, 145902

Click here to access/download
Production Data
barocaloric sco revised.docx

Click here to access/download
Production Data
Fig1.pdf

Click here to access/download
Production Data
fig2.pdf

Click here to access/download
Production Data
fig3.pdf

Click here to access/download
Production Data
fig4.pdf

Click here to access/download
Production Data
fig5.pdf

Click here to access/download
Production Data
fig6.pdf